Available online at www.sciencedirect.com
SCIENCE DIRECT®
International Journal of Solids and Structures 43 (2006) 5779–5798
INTERNATIONAL JOURNAL OF SOLIDS and STRUCTURES
www.elsevier.com/locate/ijsolstr

# Two-dimensional contact mechanics of functionally graded materials with arbitrary spatial variations of material properties

Liao-Liang Ke, Yue-Sheng Wang *

*Institute of Engineering Mechanics, Beijing Jiaotong University, Haidian District, Beijing 100044, People's Republic of China*

Received 10 May 2005; received in revised form 29 June 2005
Available online 25 August 2005

**Abstract**

A multi-layered model for frictionless contact analysis of functionally graded materials (FGMs) with arbitrarily varying elastic modulus under plane strain-state deformation has been developed. Based on the fact that an arbitrary curve can be approached by a series of continuous but piecewise linear curves, the FGM is divided into several sub-layers and in each sub-layers the shear modulus is assumed to be linear function while the Poisson's ratio is assumed to be a constant. With the model, the frictionless contact problem of a functionally graded coated half-space is investigated. By using the transfer matrix method and Fourier integral transform technique, the problem is reduced to a Cauchy singular integral equation. The contact pressure, contact region and indentation are calculated for various indenters by solving the equations numerically.


*Keywords:* Contact mechanics; Functionally graded materials; Frictionless; Plane strain state

## 1. Introduction

Functionally graded materials (FGMS) consist of a gradual change in the volume fraction of constituents from one location to the other in a component. Used as coatings and interfacial zones they tend to reduce stresses resulting from material property mismatch, increase the bonding strength, improve the surface properties and provide protection against adverse thermal and chemical environment. Thus the concept provides the materials scientists and engineers with an important tool to design new materials

* Corresponding author. Tel.: +86 10 51688417; fax: +86 10 51682094.
*E-mail address:* yswang@center.njtu.edu.cn (Y.-S. Wang).

0020-7683/$ - see front matter 
doi:10.1016/j.ijsolstr.2005.06.081

**Nomenclature**

| | |
|---|---|
| $a$, $b$ | length of contact region |
| $h_0$ | thickness of the coating |
| $m$ | slope of the triangular or wedge-shaped stamp |
| $N$ | total number of sub-layers |
| $P$ | applied normal load |
| $P_c$ | dimensionless normal load for a cylindrical stamp, $P/\mu_0 h_0$ |
| $P_t$ | dimensionless normal load for a triangular stamp, $P/\mu_0 m h_0$ |
| $P_w$ | dimensionless normal load for a wedge-shaped stamp, $P/\mu_0 m h_0$ |
| $p(x)$ | normal contact pressure |
| $p_f(x)$ | dimensionless contact pressure for a flat stamp, $p(x)/(P/2a)$ |
| $p_f(0)$ | minimum dimensionless contact pressure for a flat stamp at $x = 0$ |
| $p_c(x)$ | dimensionless contact pressure for a cylindrical stamp, $p(x)/\mu_0$ |
| $p_t(x)$ | dimensionless contact pressure for a triangular stamp, $p(x)/\mu_0 m$ |
| $p_w(x)$ | dimensionless contact pressure for a wedge-shaped stamp, $p(x)/\mu_0 m$ |
| $R$ | radius of a cylindrical stamp |
| $\overline{\mu}_i$ | shear modulus at the sub-interfaces, $i = 1, 2 \ldots, N$ |
| $\mu_0$ | shear modulus at the surface of the coating |
| $\mu^*$ | shear modulus of the homogeneous half-space |
| $\nu$ | Poisson's ratio |
| $\delta_0$ | maximum indentation depth |

for some special applications, for example, in aerospace, automobile, biomedicine, nuclear energy, gas turbine engine and many other fields. Extensive technical literatures can be found concerning the thermal stress analysis and fracture mechanics of FGMs (cf. Suresh and Mortensen, 1998).

In the past few years, some researchers began to pay attention to contact problem of functionally graded materials (FGMs). The axisymmetric problems of graded half-spaces subjected to a concentrated load or to flat, spherical and conical indenters were considered by Giannakopoulos and Suresh (1997a,b). The elastic modulus is assumed to vary in depth direction in the manner of a power function or an exponential function. In these studies, it was demonstrated that appropriate gradual variation of the elastic modulus could significantly alter the stresses around the indenter and lead to suppression of Hertzian cracking at the edge of the contact region. Later, Suresh et al. (1999), Pender and Thompson (2001), and Pender et al. (2001) draw the same conclusion. Suresh et al. (1997), Jorgensen et al. (1998) and Krumova et al. (2001) also presented the theoretical and experimental investigations of indentation testing methods to characterize the local properties of FGMs such as the elastic modulus, yield strength, strain hardening exponent, hardness and fracture toughness. Giannakopoulos and Pallot (2000) presented the closed form analytical solutions for two-dimension contact of rigid cylinders on elastic substrates which have elastic modulus varying with a power function. Edrogan and his coworkers (e.g., Dag and Erdogan, 2002; Guler and Erdogan, 2004) have developed a model where the material properties vary as exponential functions and solve the contact and coupled crack/contact problems of functionally graded coatings. It is worth mentioning the review article by Suresh (2001) on graded materials for resistance to contact deformation and damage. It was summarized that controlled gradients in mechanical properties offer opportunities for the design of surfaces with resistance to contact deformation and damage that cannot be realized in conventional homogeneous materials.

It should be noted that all those models of FGMs mentioned before assume the power function (cf. Plevako, 1973) or exponential function (cf. references cited above) of the material properties. Although

the well-known piecewise multi-layered model can simulate FGMs with arbitrarily varying properties, it introduces discontinuities of the material properties at the sub-interfaces. To overcome this disadvantage, Wang and Gross (2000) recently suggested a multi-layered model for FGMs which allows arbitrarily variation of the material properties and studied the static and dynamic crack problems under the anti-plane deformation. Based on the fact that an arbitrary curve can be approached by a series of continuous but piecewise linear curves, this model divides the FGM into a series of sub-layers with elastic modulus varying linearly in each sub-layers and continuous on the sub-interfaces. Wang et al. (2003, 2004) and Huang et al. (2003, 2004) presented detailed calculations for crack problems under both plane and anti-plane deformations to demonstrate the advantages of the model. In this paper, we will extend this model to the frictionless contact problem of a functionally graded coated half-space under plane strain-state deformation.

## 2. Fundamental solutions to a functionally graded coated half-space

### 2.1. Modelling of FGMs

Consider the problem shown in Fig. 1. A normal concentrated line force $P$ acts at the surface of a functionally graded coated half-space. The half-space is homogeneous with the shear modulus $\mu^*$ and Poisson's ratio $v^*$. Generally the shear modulus and Poisson's ratio of the functionally graded coating may be described by two arbitrary continuous functions of $y$, $\mu(y)$ and $v(y)$, with boundary values $\mu(h_0) = \mu_0$ and $v(h_0) = v_0$. In the present paper, we assume that the Poisson's ratios for both coating and half-space are a constant with the same value, that is, $v(y) = v_0 = v^* \triangleq v$. Considering the fact that an arbitrary curve can be approximated by a series of continuous but piecewise linear function, we develop a multi-layered model as shown in Fig. 2. In this model, the functionally graded coating is divided into $N$ sub-layers. The shear modulus varies linearly in each sub-layers and is continuous at the sub-interfaces, i.e.,

$$\mu(y) \approx \mu_j(y) = \overline{\mu}_j(a_j + b_j y), \quad h_j < y < h_{j-1}, \ \ j = 1, 2, \ldots, N, \tag{1}$$

where $\overline{\mu}_j$ is equal to the real value of the shear modulus at the sub-interfaces, $y = h_j$, i.e., $\overline{\mu}_j = \mu_j(h_j) = \mu(h_j)$, which leads to

$$a_j = \frac{h_{j-1} - h_j \overline{\mu}_{j-1}/\overline{\mu}_j}{h_{j-1} - h_j}, \qquad b_j = \frac{\overline{\mu}_{j-1}/\overline{\mu}_j - 1}{h_{j-1} - h_j}. \tag{2}$$

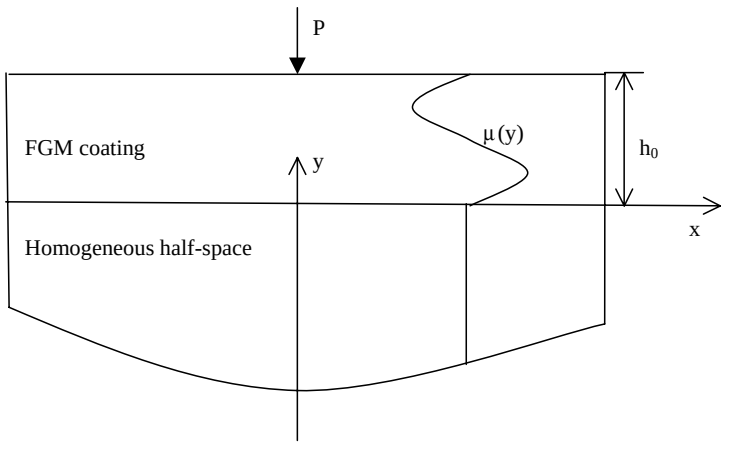


Fig. 1. A functionally graded coated half space subjected to a concentrated force $P$.

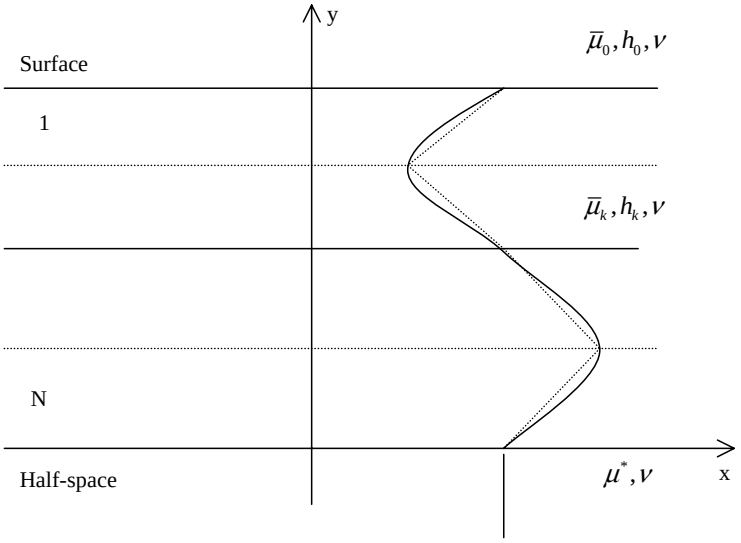


Fig. 2. The multi-layered model for the functionally graded coating.

### 2.2. Transfer matrix and displacement fundamental solutions

We consider the plane stain state of which the Hooke's law in each sub-layer is

$$\begin{aligned}
\varepsilon_{xxj} &= \frac{1-\nu}{2\mu_j}\left(\sigma_{xxj} - \frac{\nu}{1-\nu}\sigma_{yyj}\right),\\
\varepsilon_{xxj} &= \frac{1-\nu}{2\mu_j}\left(\sigma_{yyj} - \frac{\nu}{1-\nu}\sigma_{xxj}\right),\\
\gamma_{xyj} &= \frac{1}{\mu_j}\sigma_{xyj},
\end{aligned} \tag{3}$$

where $j = 1, 2, \ldots, N$. The equation of strain compatibility is

$$\frac{\partial \varepsilon_{xxj}^2}{\partial y^2} + \frac{\partial \varepsilon_{yyj}^2}{\partial x^2} = \frac{\partial \gamma_{xyj}^2}{\partial x \partial y}. \tag{4}$$

Introduce Airy stress function $F_j(x, y)$ defined as

$$\sigma_{xxj} = \frac{\partial^2 F_j}{\partial y^2}, \quad \sigma_{xyj} = -\frac{\partial^2 F_j}{\partial x \partial y}, \quad \sigma_{yyj} = \frac{\partial^2 F_j}{\partial x^2}. \tag{5}$$

Eq. (4), upon substitution of (3) and (5), yields

$$\frac{\partial^4 F_j}{\partial x^4} + 2\frac{\partial^4 F_j}{\partial x^2 \partial y^2} + \frac{\partial^4 F_j}{\partial y^4} - \frac{2\mu_j'}{\mu_j}\frac{\partial^3 F_j}{\partial y^3} - \frac{2\mu_j'}{\mu_j}\frac{\partial^3 F_j}{\partial x^2 \partial y} + \frac{2\mu_j'^2}{\mu_j^2}\frac{\partial^2 F_j}{\partial y^2} - \frac{2\mu_j'^2}{\mu_j^2}\frac{\nu}{1-\nu}\frac{\partial^2 F_j}{\partial x^2} = 0, \tag{6}$$

where the prime indicates the differentiation with respect to $y$. Applying Fourier integral transform to (6) with respect to $x$, we obtain

$$\frac{\mathrm{d}^4 \widetilde{F}_j}{\mathrm{d}y^4} - 2s^2\frac{\mathrm{d}^2 \widetilde{F}_j}{\mathrm{d}y^2} + s^4 \widetilde{F}_j - \frac{2b_j}{a_j + b_j y}\frac{\mathrm{d}^3 \widetilde{F}_j}{\mathrm{d}y^3} + \frac{2b_j s^2}{a_j + b_j y}\frac{\mathrm{d}\widetilde{F}_j}{\mathrm{d}y} + \frac{2b_j^2}{(a_j + b_j y)^2}\frac{\mathrm{d}^2 \widetilde{F}_j}{\mathrm{d}y^2} + \frac{\nu}{1-\nu}\frac{2b_j^2 s^2}{(a_j + b_j y)^2}\widetilde{F}_j = 0, \tag{7}$$

where "~" indicates the Fourier transform. Introduce the substitutes

$$\xi_j = 2s(a_j + b_j y)/b_j, \qquad \widetilde{F}_j = \varphi(\xi_j)\xi_j/2. \tag{8}$$

Eq. (7) reduces to a Whittaker equation (Slater, 1960)

$$\frac{\mathrm{d}^4\varphi_j}{\mathrm{d}\xi_j^4} + \frac{2}{\xi_j}\frac{\mathrm{d}^3\varphi_j}{\mathrm{d}\xi_j^3} - \left(\frac{1}{2} + \frac{4}{\xi_j^2}\right)\frac{\mathrm{d}^2\varphi_j}{\mathrm{d}\xi_j^2} + \left(\frac{4}{\xi_j^3} - \frac{1}{2\xi_j}\right)\frac{\mathrm{d}\varphi_j}{\mathrm{d}\xi_j} + \left(\frac{1}{16} + \frac{1-\gamma^2}{\xi_j^2}\right)\varphi_j = 0, \tag{9}$$

where $\gamma = \sqrt{(1-2v)/(2-2v)}$. The solution of (9) can be written as (Slater, 1960)

$$\varphi_j = A_{j1}W_{\gamma,1.5}(\xi_j) + A_{j2}W_{-\gamma,1.5}(\xi_j) + A_{j3}W_{\gamma,1.5}(-\xi_j) + A_{j4}W_{-\gamma,1.5}(-\xi_j), \tag{10}$$

where $A_{jl}$ $(l = 1,2,3,4)$ are unknown coefficients; and $W_{\pm\gamma,1.5}(\pm\xi_j)$ are Whittaker functions. Inserting Eq. (10) into (8), we obtain the transformed Airy stress function in each sub-layer as

$$\begin{aligned}\widetilde{F}_j &= (A_{j1}W_{\gamma,1.5}(\xi_j) + A_{j2}W_{-\gamma,1.5}(\xi_j) + A_{j3}W_{\gamma,1.5}(-\xi_j) + A_{j4}W_{-\gamma,1.5}(-\xi_j))\xi_j/2 \\ &\triangleq A_{j1}\tilde{\varphi}_{j1}(\xi_j) + A_{j2}\tilde{\varphi}_{j2}(\xi_j) + A_{j3}\tilde{\varphi}_{j3}(\xi_j) + A_{j4}\tilde{\varphi}_{j4}(\xi_j).\end{aligned} \tag{11}$$

From (5) and the strain–displacement relations, one may obtain the Fourier transforms of the displacement and stress components which may be written as the matrix form

$$\{S_j\} = [T_j(y)]\{A_j\} = [T_{j1}(y), T_{j2}(y), T_{j3}(y), T_{j4}(y)]\{A_j\}, \tag{12}$$

where

$$\begin{aligned}\{S_j\} &= [\tilde{u}_{xj}, \tilde{u}_{yj}, \tilde{\sigma}_{xyj}, \tilde{\sigma}_{yyj}]^{\mathrm{T}}, \\ \{A_j\} &= [A_{j1}, A_{j2}, A_{j3}, A_{j4}]^{\mathrm{T}}, \\ [T_{jl}(y)] &= [T_{jl1}(y), T_{jl2}(y), T_{jl3}(y), T_{jl4}(y)]^{\mathrm{T}},\end{aligned}$$

with

$$\begin{aligned}T_{jl1}(y) &= -\frac{\mathrm{i}(1-v)}{2\mu_j(y)s}\frac{\mathrm{d}^2\tilde{\varphi}_{jl}}{\mathrm{d}y^2} - \frac{\mathrm{i}vs}{2\mu_j(y)}\tilde{\varphi}_{jl}, \\ T_{jl2}(y) &= \frac{1-v}{2\mu_j(y)s^2}\frac{\mathrm{d}^3\tilde{\varphi}_{jl}}{\mathrm{d}y^3} - \frac{\overline{\mu}_j b_j(1-v)}{2\mu_j^2(y)s^2}\frac{\mathrm{d}^2\tilde{\varphi}_{jl}}{\mathrm{d}y^2} - \frac{2-v}{2\mu_j(y)}\frac{\mathrm{d}\tilde{\varphi}_{jl}}{\mathrm{d}y} - \frac{\overline{\mu}_j b_j v}{2\mu_j^2(y)}\tilde{\varphi}_{jl}, \\ T_{jl3}(y) &= -\mathrm{i}s\frac{\mathrm{d}\tilde{\varphi}_{jl}}{\mathrm{d}y}, \quad T_{jl4}(y) = -s^2\tilde{\varphi}_{jl}, \qquad l = 1,2,3,4\end{aligned}$$

and the superscript "T" denoting transposition of matrix.

In the homogeneous half-space, the Airy stress functions satisfy the biharmonic equation

$$\nabla^4 F_{N+1} = 0. \tag{13}$$

Following the similar process, we get

$$\{S_{N+1}\} = [T_{N+1}(y)]\{A_N\}, \tag{14}$$

where $\{A_{N+1}\} = [A_{N+1,1}, A_{N+1,2}]^{\mathrm{T}}$ and

$$[T_{N+1}(y)] = \begin{bmatrix} s/2\mathrm{i}\mu^* & -|s|/2\mu^* & -\mathrm{i}s & -s^2 \\ [ys + 2(1-v)|s|/s]/2\mathrm{i}\mu^* & (1-2v-y|s|)/2\mu^* & -\mathrm{i}s(y|s|+1) & -s^2 y \end{bmatrix}^{\mathrm{T}} \mathrm{e}^{|s|y}. \tag{15}$$

The stresses and displacements are continuous at the sub-interfaces, $y = h_j$, which states

$$\begin{aligned} &\sigma_{xyj} - \sigma_{xyj+1} = 0, \\ &\sigma_{yyj} - \sigma_{yyj+1} = 0, \\ &u_{xj} - u_{xj+1} = 0, \\ &u_{yj} - u_{yj+1} = 0 \end{aligned} \tag{16}$$

and along the coating surface, $y = h_0$, we have

$$\begin{aligned} &\sigma_{xy0}(x, h_0) = 0, \\ &\sigma_{yy0}(x, h_0) = -\delta(x)P. \end{aligned} \tag{17}$$

where $\delta(\cdot)$ is the delta function. In the transformed domain, the boundary conditions (16) and (17) may be written as

$$\{S_j\} - \{S_{j+1}\} = 0, \quad y = h_j, \qquad j = 1, 2, \ldots, N, \tag{18}$$

$$[B_1][T_1(h_0)]\{A_1\} = \{0, -P\}^{\mathrm{T}}, \tag{19}$$

where

$$[B_1] = \begin{bmatrix} 0 & 0 & 1 & 0 \\ 0 & 0 & 0 & 1 \end{bmatrix}.$$

The above Eqs. (18) and (19) is a recurrence relation which, upon substitution (12) and (14), may yield the expression of $\{A_j\}$ in terms of $\{0, P\}^{\mathrm{T}}$,

$$\{A_j\} = -[\overline{V}_{j-1}][\overline{V}_N][K]^{-1}\{0, P\}^{\mathrm{T}}, \quad j = 1, 2, \ldots, N, \tag{20}$$

where

$$\begin{aligned} &[V_j] = [T_j(h_j)]^{-1}[T_{j+1}(h_j)], \quad [\overline{V}_j] = [V_0][V_1][V_2]\cdots[V_N], \qquad j \geqslant 1, \\ &[K] = [B_1][T_1(h_0)][\overline{V}_N], \qquad [\overline{V}_0] = [V_0]. \end{aligned}$$

Substituting (20) into (12) and taking the inverse Fourier transform, we have

$$[u_{xj}, u_{yj}, \sigma_{xyj}, \sigma_{yyj}]^{\mathrm{T}} = \frac{1}{2\pi}\int_{-\infty}^{\infty}[M]\{0, P\}^{\mathrm{T}}\mathrm{e}^{\mathrm{i}sx}\,\mathrm{d}s, \tag{21}$$

where we have denoted

$$[M(s, y)] = -[T_j(y)][\overline{V}_{J-1}][\overline{V}_N][K]^{-1},$$

which is the transfer matrix of the multiple layered medium with the normal force. Extracting the displacement components at $y = h_0$ from Eq. (21), we have

$$[u_{x0}, u_{y0}]^{\mathrm{T}} = \frac{1}{2\pi}\int_{-\infty}^{\infty} m(s, h_0)\{0, P\}^{\mathrm{T}}\mathrm{e}^{\mathrm{i}sx}\,\mathrm{d}s, \tag{22}$$

where

$$m(s, h_0) = [B_2][M(s, h_0)], \quad [B_2] = \begin{bmatrix} 1 & 0 & 0 & 0 \\ 0 & 1 & 0 & 0 \end{bmatrix}.$$

Considering the asymptotic behavior of Whittaker functions for large arguments (Slater, 1960), one may easily prove

$$\lim_{s\to+\infty} sm(s,h_0)=\begin{bmatrix}\alpha_1 & -\mathrm{i}\alpha_2\\ \mathrm{i}\alpha_2 & \alpha_1\end{bmatrix}, \tag{23}$$

where

$$\alpha_1=\frac{v-1}{\mu_0},\qquad \alpha_2=\frac{2v-1}{2\mu_0}.$$

Rewrite Eq. (22) as

$$[u_{x0},u_{y0}]^{\mathrm{T}}=\frac{1}{2\pi}\int_{-\infty}^{\infty}\Lambda\{0,P\}^{\mathrm{T}}\mathrm{e}^{\mathrm{i}sx}\,\mathrm{d}s+\frac{1}{2\pi}\int_{-\infty}^{\infty}[m(s,h_0)-\Lambda]\{0,P\}^{\mathrm{T}}\mathrm{e}^{\mathrm{i}sx}\,\mathrm{d}s, \tag{24}$$

where

$$\Lambda=\frac{1}{s}\begin{bmatrix}\mathrm{sign}(s)\alpha_1 & -\mathrm{i}\alpha_2\\ \mathrm{i}\alpha_2 & \mathrm{sign}(s)\alpha_1\end{bmatrix}.$$

If we consider the following properties of the elements of the matrix $m(s)$:

$$m_{ij}(-s)=(-1)^{i+j}m_{ij}(s),\quad i,j=1,2 \tag{25}$$

and use the relations

$$\int_0^{\infty}\frac{\cos(sx)}{s}\,\mathrm{d}s=-\ln|x|,\qquad \int_0^{\infty}\frac{\sin(sx)}{s}\,\mathrm{d}s=\frac{\pi}{2}\,\mathrm{sign}(x), \tag{26}$$

we can obtain the surface displacement components from Eq. (22)

$$u_{x0}(x)=\frac{\alpha_2 P}{2}\,\mathrm{sign}(x)+\frac{P}{\pi}\int_0^{\infty}[\mathrm{i}m_{12}(s)-\alpha_2/s]\sin(sx)\,\mathrm{d}s, \tag{27}$$

$$u_{y0}(x)=-\frac{\alpha_1 P}{\pi}\ln|x|+\frac{P}{\pi}\int_0^{\infty}[m_{22}(s)-\alpha_1/s]\cos(sx)\,\mathrm{d}s. \tag{28}$$

It should be noted that the logarithmic singularity involved in the displacements makes the deformation indeterminant (i.e., the surface cannot be used as reference for zero displacements, (cf. Johnson, 1985)). For a homogeneous half-space without the functionally graded coating, the second terms including the integrals in Eqs. (27) and (28) vanish, and then we get the results presented in Johnson (1985).

## 3. Stamp problems for a functionally graded coated half-space

The previous section gives the fundamental solutions to a functionally graded coated half-space subjected to a concentrated line load. We will show in this section how to use the fundamental solution (28) to solve the contact problems of rigid stamps as shown in Fig. 3. This is a typical mixed boundary value problems in which the displacement components are known through the given stamp profiles within the contact region, $-b\leqslant x\leqslant a$, and the surface traction is known to be zero outside the contact region. Suppose the normal contact pressure is $p(x)$, and then the superposition theorem gives the normal displacement component of the surface

$$u_{y0}(x)=-\frac{\alpha_1}{\pi}\int_{-b}^{a}\ln|x-t|p(t)\,\mathrm{d}t+\frac{1}{\pi}\int_{-b}^{a}p(t)I(x,t)\,\mathrm{d}t, \tag{29}$$

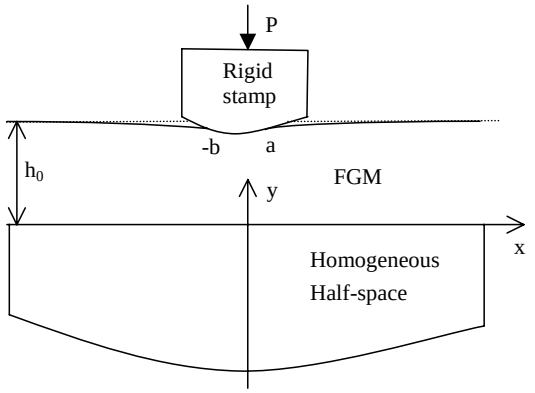


Fig. 3. Geometry of the contact problem.

where

$$I(x,t)=\int_0^\infty [m_{22}(s)-\alpha_1/s]\cos[s(x-t)]\,\mathrm{d}s. \tag{30}$$

Derivation of Eq. (29) with respect to $x$ yields

$$\frac{\alpha_1}{\pi}\int_{-b}^{a}\frac{p(t)}{t-x}\,\mathrm{d}t+\frac{1}{\pi}\int_{-b}^{a}p(t)Q(x,t)\,\mathrm{d}t=g(x), \tag{31}$$

where

$$\begin{aligned} g(x)&=\frac{\partial u_{y0}(x)}{\partial x},\\ Q(x,t)&=\frac{\partial I(x,t)}{\partial x}=-\int_0^\infty [sm_{22}(s)-\alpha_1]\sin[s(x-t)]\,\mathrm{d}s. \end{aligned} \tag{32}$$

Eq. (31) is a Cauchy singular integral equation for the unknown contact pressure $p(x)$, provided that the stamp profile $u_{y0}(x)$ $(-b<x<a)$ is prescribed. The static equilibrium for the contact pressure $p(x)$ must satisfy, which yields an additional condition for uniqueness of the solution

$$\int_{-b}^{a}p(t)\,\mathrm{d}t=P. \tag{33}$$

By introducing the following normalized quantities:

$$t=\frac{a+b}{2}\eta+\frac{a-b}{2},\quad x=\frac{a+b}{2}\varsigma+\frac{a-b}{2},\qquad -b<(t,x)<a,\ -1<(\eta,\varsigma)<1, \tag{34}$$

the Cauchy singular equation (31) and Eq. (33) may be expressed in the following form:

$$\frac{\alpha_1}{\pi}\int_{-1}^{1}\frac{p(\eta)}{\eta-\varsigma}\,\mathrm{d}\eta+\frac{a+b}{2\pi}\int_{-1}^{1}p(\eta)Q(\varsigma,\eta)\,\mathrm{d}\eta=g(\varsigma), \tag{35}$$

$$\int_{-1}^{1}p(\eta)\,\mathrm{d}\eta=2P/(a+b), \tag{36}$$

where we have simply denoted $p(t)=p(\eta)$, $Q(x,t)=Q(\varsigma,\eta)$ and $g(x)=g(\varsigma)$ with consideration of Eq. (34). These equations can be solved numerically by following the method developed by Erdogan and Gupta (1972) or Krenk (1975). To this end, one should first examine the singular behavior of $p(\eta)$ at $\eta=\pm1$

(i.e., the ends of the contact region, $-b$ and $a$). Generally speaking, if the contact is smooth at one end, the pressure at this end is zero; otherwise it has inverse square root singularity at this end. If both ends of the contact region are smooth, a consistency condition should be considered (Muskhelishvili, 1953). This will be discussed in the next section for particular examples.

## 4. Examples

A few typical stamp problems will be formulated in this section based on the previous analysis. Numerical results and discussion will be presented in the next section.

### 4.1. Frictionless rigid flat stamp

Consider the contact problem for a FGM coated half-space shown in Fig. 4 where the stamp is flat, that is

$$u_{y0}(x) = \text{constant}, \qquad \frac{\partial u_{y0}(x)}{\partial x} = 0. \tag{37}$$

In this case, we have

$$g(\varsigma) = 0, \qquad b = a. \tag{38}$$

Eqs. (35) and (36), with consideration of Eq. (38), can be solved numerically by the method of Erdogan and Gupta (1972). Notice that the function $p(\eta)$ has integrable singularities at $\eta = \pm 1$. We can express them as

$$p(\eta) = \frac{f(\eta)}{\sqrt{1-\eta^2}} \tag{39}$$

and then Eqs. (35) and (36) reduce to (Erdogan and Gupta, 1972)

$$\frac{1}{M}\sum_{l=1}^{M} f(\eta_l)\left[\frac{\alpha_1}{\eta_l - \varsigma_r} + aQ(a\varsigma_r, a\eta_l)\right] = 0, \tag{40a}$$

$$\frac{1}{M}\sum_{l=1}^{M} f(\eta_l) = \frac{P}{a\pi}, \tag{40b}$$

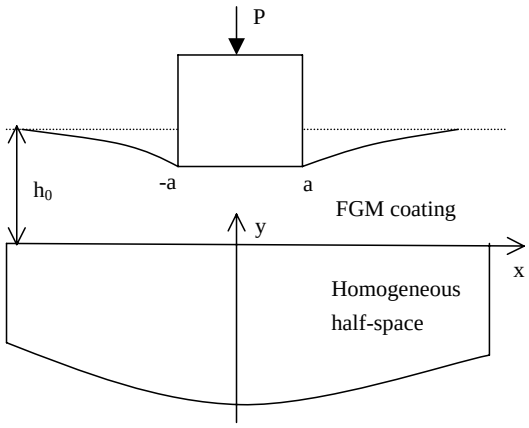


Fig. 4. Geometry of the flat stamp problem.

where $\eta_l = \cos[(2l-1)\pi/2M]$, $\varsigma_r = \cos[\pi r/M]$, $r = 1, 2, \ldots, M-1$, and $M$ is the total number of the discrete points of $f(\eta_l)$ in $(-1, 1)$. Eqs. (40a,b) provide a system of $M$ equations to determine $M$ unknowns, $f(\eta_1), \ldots, f(\eta_M)$.

### 4.2. Frictionless rigid cylindrical stamp

Consider the cylindrical stamp problem shown in Fig. 5 where the stamp profile is given by

$$u_{y0}(x) = \left(R - \sqrt{R^2 - x^2}\right) - \delta_0, \quad \frac{\partial u_{y0}(x)}{\partial x} = \frac{x}{\sqrt{R^2 - x^2}}, \qquad -a \leqslant x \leqslant a, \tag{41}$$

where $R$ is the radius of the stamp; $a$ is the semi-length of the contact region; and $\delta_0$ is the maximum indentation depth appearing at $x = 0$. $\delta_0$ and $a$ are undetermined. In the absence of adhesion, the analysis requires the additional condition that the contact pressure must be zero at the ends of the contact region, i.e.,

$$p(\pm a) = 0, \tag{42}$$

therefore, the semi-length of the contact region, $a$, becomes a function of the applied normal line load $P$. For the cylindrical stamp, we have

$$g(\varsigma) = \frac{a\varsigma}{\sqrt{R^2 - (a\varsigma)^2}}, \quad b = a. \tag{43}$$

It is noted that for the cylindrical stamp the solution of Eqs. (35) and (36) must satisfy a consistency condition (Muskhelishvili, 1953),

$$\int_{-1}^{1} \frac{S(\varsigma)\,\mathrm{d}\varsigma}{\sqrt{(1-\varsigma^2)}} = 0, \tag{44}$$

where

$$S(\varsigma) = \frac{\alpha_1}{\pi} \int_{-1}^{1} \frac{p(\eta)}{\eta - \varsigma}\,\mathrm{d}\eta.$$

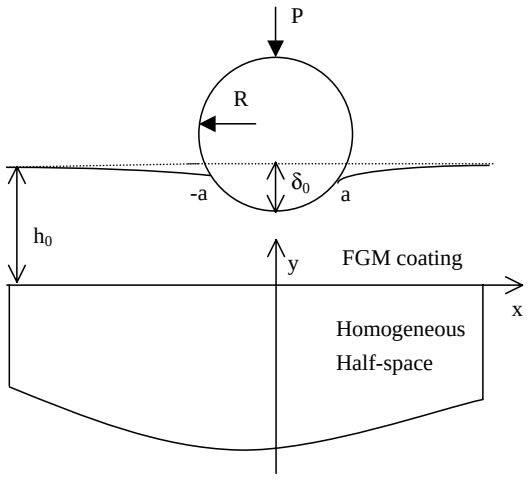


Fig. 5. Geometry of the cylindrical stamp problem.

Referring to Erdogan and Gupta (1972), it is easily proved that Eq. (44) is an identity. Then, Eqs. (35) and (36), with consideration of Eq. (43), can be solved numerically by the method of Erdogan and Gupta (1972). Expressed $p(\eta)$ as

$$p(\eta) = f(\eta)\sqrt{1-\eta^2}, \tag{45}$$

then Eqs. (35) and (36) reduce to (Erdogan and Gupta, 1972)

$$\sum_{l=1}^{M} \frac{(1-\eta_l^2)f(\eta_l)}{(M+1)}\left[\frac{\alpha_1}{\eta_l-\varsigma_r} + aQ(\varsigma_r,\eta_l)\right] = \frac{a\varsigma_r}{\sqrt{R^2-(a\varsigma_r)^2}}, \tag{46a}$$

$$\sum_{l=1}^{M} \frac{(1-\eta_l^2)f(\eta_l)}{(M+1)} = \frac{P}{a\pi}, \tag{46b}$$

where $\eta_l = \cos[l\pi/(M+1)]$, $\varsigma_r = \cos[\pi(2r-1)/2(M+1)]$, $r = 1,2,\ldots,M+1$, and $M$ is the total number of the discrete points of $f(\eta_l)$ in $(-1,1)$.

It is noted that there are $M+2$ equations for $M+1$ unknowns, $f(\eta_1),\ldots,f(\eta_M)$ and $a$. As in Erdogan and Gupta (1972), we choose $M$ from $M+1$ equations in (46a). In practice, we can select $M$ as an even integer and ignore the equation corresponding to $r = M/2+1$.

### 4.3. Frictionless rigid triangular stamp

Consider the triangular stamp problem shown in Fig. 6 where the stamp profile is given by

$$u_{y0}(x) = mx + c, \quad \frac{\partial u_{y0}(x)}{\partial x} = m, \qquad m > 0. \tag{47}$$

In this case, we have

$$g(\varsigma) = m, \qquad b = 0. \tag{48}$$

Eqs. (35) and (36), with consideration of Eq. (48), can be solved numerically by the method of Krenk (1975). Notice that the triangular stamp has a sharp corner at $x = 0$ and smooth contact at $x = a$. We can expressed $p(\eta)$ as

$$p(\eta) = f(\eta)\sqrt{(1-\eta)/(1+\eta)}. \tag{49}$$

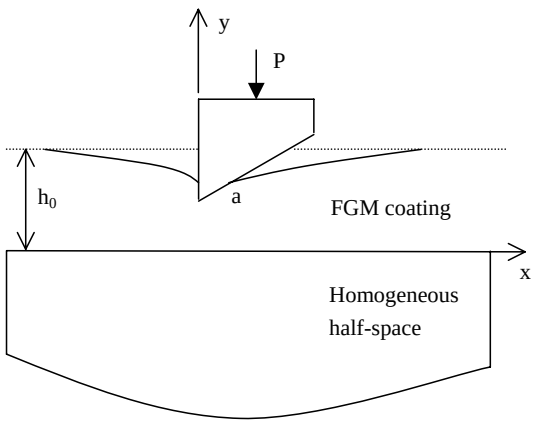


Fig. 6. Geometry of the triangular stamp problem.

Then Eqs. (35) and (36) reduce to (Krenk, 1975)

$$\sum_{l=1}^{M} W_l^M f(\eta_l)\left[\frac{\alpha_1}{\eta_l-\varsigma_r}+\frac{a}{2}Q(\varsigma_r,\eta_l)\right]=m, \tag{50a}$$

$$\sum_{l=1}^{M} W_l^M f(\eta_l)=\frac{2P}{a\pi}, \tag{50b}$$

where $M$ is the total number of the discrete points of $f(\eta_l)$ in $(-1,1)$; $\eta_l$, $\varsigma_r$ and $W_l^M$ are, respectively, determined by

$$P_M^{(\alpha,\beta)}(\eta_l)=0, \quad l=1,2,\ldots,M, \tag{51}$$

$$P_M^{(-\alpha,-\beta)}(\varsigma_r)=0, \quad l=1,2,\ldots,M, \tag{52}$$

$$W_l^M=-2^{-(\alpha+\beta)}\frac{\Gamma(\alpha)\Gamma(1-\alpha)}{\pi}\frac{P_{M+\alpha+\beta}^{(-\alpha,-\beta)}(\eta_l)}{P_M^{(\alpha,\beta)'}(\eta_l)}, \tag{53}$$

where $\alpha=-\beta=1/2$; $\Gamma(\,)$ is the Gamma function; and $P_M^{(\alpha,\beta)}(\,)$ is the Jacobi polynomial of degree $M$.

It is noted that one end of the contact region, namely $a$ is unknown. However, Eqs. (50a,b) provide $M+1$ equations to determine $f(\eta_1),\ldots,f(\eta_M)$ and $a$.

### 4.4. Frictionless rigid wedge-shaped stamp

Consider the wedge-shaped stamp problem shown in Fig. 7 where the stamp profile is given by

$$u_{y0}(x)=mx\,\mathrm{sign}(x)+c, \quad \frac{\partial u_{y0}(x)}{\partial x}=m\,\mathrm{sign}(x), \qquad -a<x<a. \tag{54}$$

In this case, we have

$$g(\varsigma)=\mathrm{sign}(\varsigma)m, \qquad b=a. \tag{55}$$

It is noted that $g(\varsigma)$ presents a jump discontinuity at $\varsigma=0$ (i.e., $x=0$). Therefore, the method developed Erdogan and Gupta (1972) and Krenk (1975) cannot be used directly to solve Eqs. (35) and (36) in the present case. Here we employ the method of Ioakimidis (1980). Set

$$p(\eta)=h(\eta)+\psi(\eta), \tag{56}$$

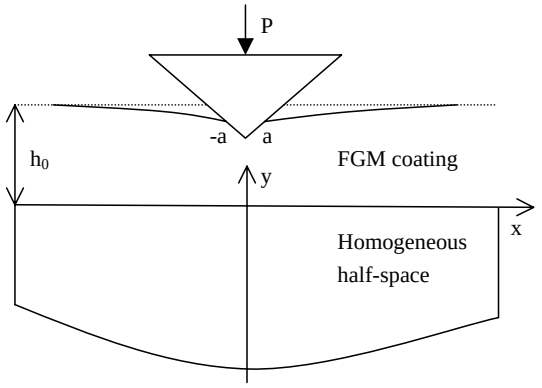


Fig. 7. Geometry of the wedge-shaped stamp problem.

where $\psi(\eta)$ is an unknown function to be determined, and $h(\eta)$ satisfies

$$\frac{\alpha_1}{\pi}\int_{-1}^{1}\frac{h(\eta)}{\eta-\varsigma}\,\mathrm{d}\eta = g(\varsigma) \tag{57}$$

of which the closed-form solution is given by

$$h(\eta) = \frac{m}{\alpha_1\pi}\ln\frac{1+\sqrt{1-\eta^2}}{1-\sqrt{1-\eta^2}}. \tag{58}$$

Substitution of Eq. (56) into Eqs. (35) and (36) with consideration of Eqs. (57) and (58) yields

$$\frac{\alpha_1}{\pi}\int_{-1}^{1}\frac{\psi(\eta)}{\eta-\varsigma}\,\mathrm{d}\eta + \frac{a}{\pi}\int_{-1}^{1}\psi(\eta)Q(\varsigma,\eta)\,\mathrm{d}\eta = F(\varsigma), \tag{59}$$

$$\int_{-1}^{1}\psi(\eta)\,\mathrm{d}\eta = \tau_0, \tag{60}$$

where

$$F(\varsigma) = -\frac{a}{\pi}\int_{-1}^{1}h(\eta)Q(\varsigma,\eta)\,\mathrm{d}\eta,$$

$$\tau_0 = \frac{P}{a} - \int_{-1}^{1}h(\eta)\,\mathrm{d}\eta = \frac{P}{a} - \frac{2m}{\alpha_1}.$$

The numerical method of Erdogan and Gupta (1972) can be directly applied to the solution of Eqs. (59) and (60). Expressed $\psi(\eta)$ as

$$\psi(\eta) = f(\eta)\sqrt{1-\eta^2}. \tag{61}$$

Then Eqs. (59) and (60) reduce to (Erdogan and Gupta, 1972)

$$\sum_{l=1}^{M}\frac{(1-\eta_l^2)f(\eta_l)}{(M+1)}\left[\frac{\alpha_1}{\eta_l-\varsigma_r} + aQ(\varsigma_r,\eta_l)\right] = F(\varsigma_r), \tag{62a}$$

$$\sum_{l=1}^{M}\frac{(1-\eta_l^2)f(\eta_l)}{(M+1)} = \frac{\tau_0}{\pi}, \tag{62b}$$

where $\eta_l = \cos[l\pi/(M+1)]$, $\varsigma_r = \cos[\pi(2r-1)/2(M+1)]$, $r = 1,2,\ldots,M+1$, and $M$ is the total number of the discrete points of $f(\eta_l)$ in $(-1,1)$. As in the case of the cylindrical stamp, one can select $M$ from $M+1$ equations in (62a) and combine them with (62b) to get $M+1$ unknowns, $f(\eta_l)$ $(l = 1,2,\ldots,M)$ and $a$.

## 5. Numerical results and discussion

To verify the effectiveness of the present model, we first consider the frictionless contact of rigid stamps, by assuming the shear modulus of the coating varying in the exponential manner

$$\mu(y) = \mu^* e^{\lambda(y/h_0)}, \tag{63}$$

where $\lambda = \log(\mu_0/\mu^*)$ and $\mu^*$ is the shear modulus of the homogeneous half-space. Throughout the paper the Possion's ratio is taken as $\nu = 0.3$. Guler and Erdogan (2004) have studied the contact of flat and triangular stamps by taking the same form as Eq. (63) for the shear modulus of the coating. Here we solve the same problem using the present model for comparison with Guler and Erdogan's method. And in addition, the cylindrical and wedge-shaped stamps are also considered here.

For the use of the present model, we have to first determine how many sub-layers are necessary to obtain the sufficiently accurate results. To this end, we calculate the minimum dimensionless contact pressure, $p_f(0)$, of the flat stamp with $\mu^*/\mu_0 = 8$, $a/h_0 = 0.1$ and 0.5 for different values of $N$ as shown in Table 1. We can see that with the increase of $N$, the results are increasingly close to each other. And the results with $N = 4$ or 6 may be considered sufficiently accurate. So we could choose $N = 6$, that is, divide the coating into six sub-layers.

In order to compare the present model to Guler and Erdogan's, we choose the same materials parameters as in Guler and Erdogan (2004), and calculate the contact pressure for various kinds of stamps. Figs. 8–11 present the non-dimensioned contact pressure, i.e., $p_f(x)$, $p_c(x)$, $p_t(x)$, $p_w(x)$, obtained by the present model and Gular and Erdogan's method for the flat, cylindrical, triangular and wedge-shaped stamps for various values of the stiffness ratio $\mu^*/\mu_0$ with the fixed value of $a/h_0$, respectively. Among them the results for the flat and triangular stamps have been presented by Guler and Erdogan (2004). Good agreement is shown between the results of the present model and those of Guler and Erdogan. It is noted that Guler and Erdogan's analysis only allows for exponential variation of the shear modulus, while ours has no such limitation.

Some features may be observed from Figs. 8–11. For instance, the contact pressure has singularity at both ends $x = \pm a$ for the flat stamp (Fig. 8), but at one end $x = 0$ for the triangular stamp (Fig. 10). Also singularity is seen near the tip $x = 0$ of the wedge-shaped stamp (Fig. 11). However, smooth contact is shown at both ends for the cylindrical (Fig. 9) and wedge-shaped (Fig. 11) stamps, and at one end for the triangular stamp (Fig. 10). The singularity of the contact ends has been discussed in previous Section

Table 1
Effect of $N$ on the minimum dimensionless contact pressure of the flat stamp with $\mu^*/\mu_0 = 8$, $a/h_0 = 0.1$ and 0.5

| $-N$ | $a/h_0 = 0.1$ | $a/h_0 = 0.5$ |
|---|---|---|
| | $p_f(0)$ | $p_f(0)$ |
| 2 | −0.71831 | −0.80957 |
| 4 | −0.70709 | −0.81105 |
| 6 | −0.70476 | −0.81123 |
| 8 | −0.70477 | −0.81125 |

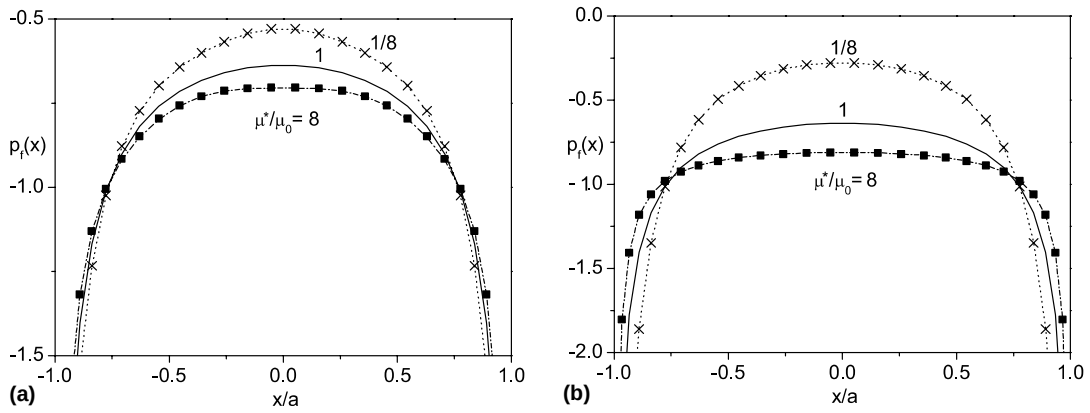


Fig. 8. The distribution of the contact pressure on the surface of FGM coating loaded by a flat stamp for various values of the stiffness ratio $\mu^*/\mu_0$: (a) $a/h_0 = 0.1$ and (b) $a/h_0 = 0.5$. The lines are from the present results and the scattered symbols from Guler and Erdogan's results.

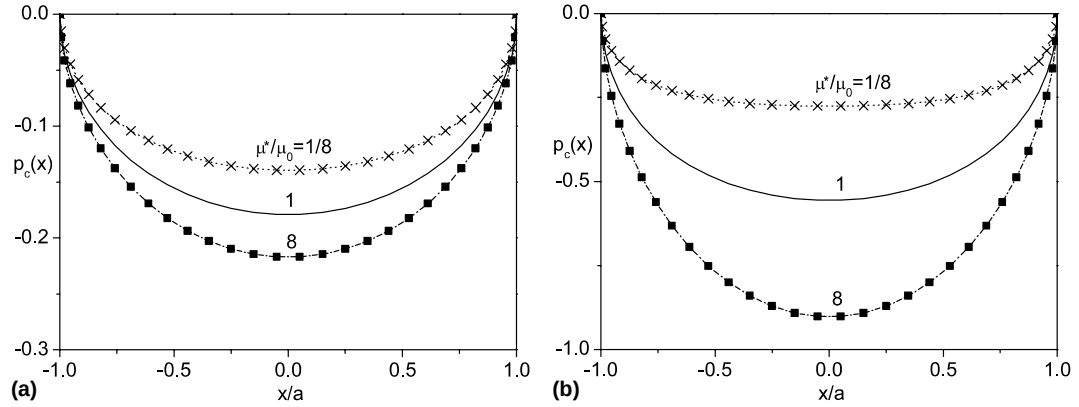


Fig. 9. The distribution of the contact pressure on the surface of FGM coating loaded by a cylindrical stamp for various values of the stiffness ratio $\mu^*/\mu_0$, $R/h_0 = 0.8$: (a) $a/h_0 = 0.1$ and (b) $a/h_0 = 0.3$. The lines are from the present results and the scattered symbols from Guler and Erdogan's results.

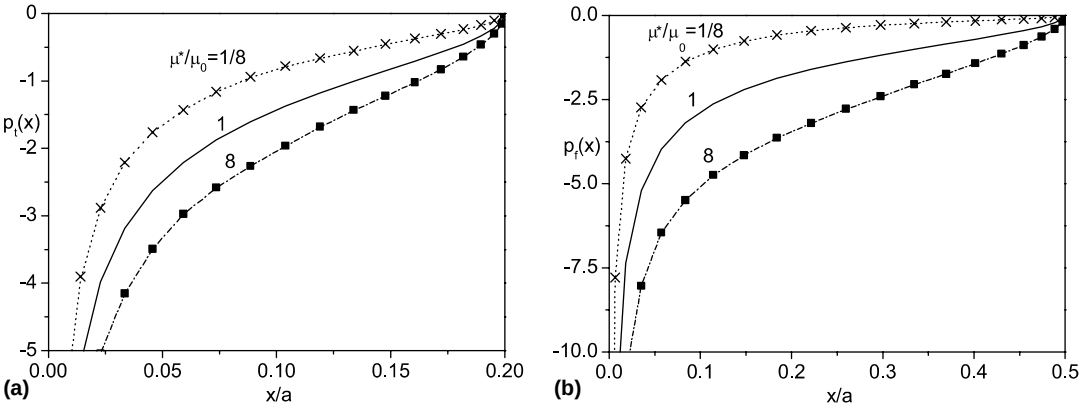


Fig. 10. The distribution of the contact pressure on the surface of FGM coating loaded by a triangular stamp for various values of the stiffness ratio $\mu^*/\mu_0$: (a) $a/h_0 = 0.2$ and (b) $a/h_0 = 0.5$. The lines are from the present results and the scattered symbols from Guler and Erdogan's results.

4 for the four kinds of the stamps considered here. The numerical results demonstrate the analytical results therein. The same singular behavior is also involved in contact of the homogeneous elastic solids.

Effects of the stiffness ratio $\mu^*/\mu_0$ (or equivalently, the exponential index $\lambda$) on the contact pressure are shown obviously in Figs. 8–11 for the case of the fixed contact region (i.e., the value of $a/h_0$). With the increase of $\mu^*/\mu_0$, the contact pressure for the flat stamp decreases and becomes more even in most part of the contact area, but it increases in the area near two ends; while the contact pressure for the other three kinds of stamps increases in all contact area and becomes more uneven. This behavior provides a way for us to change the distribution of the contact pressure by adjusting the stiffness of the coating surface (or equivalently adjusting the gradient of the coating).

As well known, indentation-testing methods can be used to characterize the local properties of FGMs such as the elastic modulus, yield strength, strain hardening exponent, hardness and fracture toughness. Therefore we calculate the contact region $a$ and the maximum indentation depth $\delta_0$ for the cylindrical

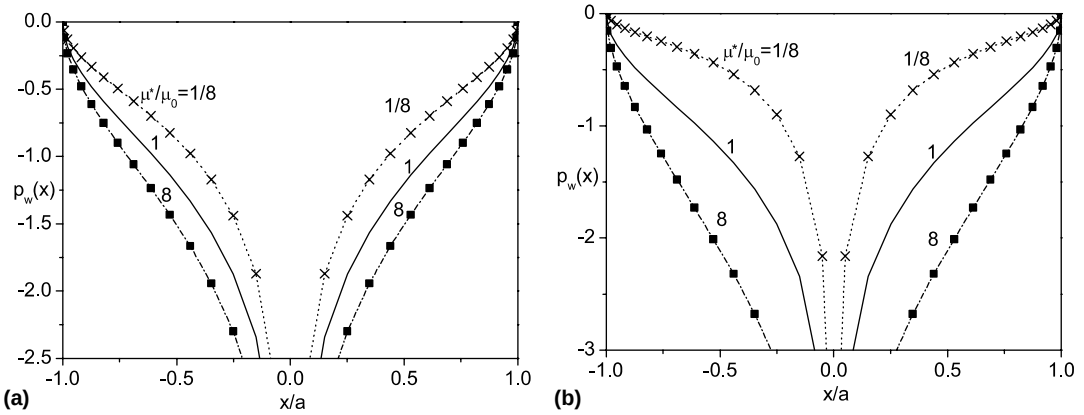


Fig. 11. The distribution of the contact pressure on the surface of FGM coating loaded by a wedge-shaped stamp for various values of the stiffness ratio $\mu^*/\mu_0$: (a) $a/h_0 = 0.1$ and (b) $a/h_0 = 0.3$. The lines are from the present results and the scattered symbols from Guler and Erdogan's results.

and wedge-shaped stamps. Throughout the paper the indentation is defined the vertical displacement with respective to the value at $x = 5h_0$. That is to say, the maximum indentation depth $\delta_0$ is difference between the vertical displacements at $x = 0$ and $x = 5h_0$, i.e., $\delta_0 = u_{y0}(0) - u_{y0}(5h_0)$. The relations of $P$ vs $a$ and $P$ vs $\delta_0$ are shown in Figs. 12 and 13 for various values of the stiffness ratio $\mu^*/\mu_0$. For the cylindrical stamp, the $P_c$–$a$ curves (Fig. 12a) are concave, while the $P_c$–$\delta_0$ curves (Fig. 12b) are slight concave for smaller $P_c$ but are almost straight for larger $P_c$. For the wedge-shaped stamp, the $P_w$–$a$ curves (Fig. 13a) are concave for $\mu^* > \mu_0$ but are convex for $\mu^* < \mu_0$ (and is straight for $\mu^* = \mu_0$), while the $P_w$–$\delta_0$ curves (Fig. 13b) are concave for larger values of $\mu^*/\mu_0$ but are almost straight for smaller values of $\mu^*/\mu_0$. Both Figs. 12 and 13 show that the larger applied normal load is needed for the stiffer coating surface than for the softer one to create the same contact region ($a$) and the same maximum indentation depth $\delta_0$. The dependence of $P$–$\delta_0$ curves on the stiffness ratio $\mu^*/\mu_0$ (or equivalently, the exponential index $\lambda$) provides a way for us to measure the stiffness of the coating surface and the gradient of the coating using the indentation-testing method.

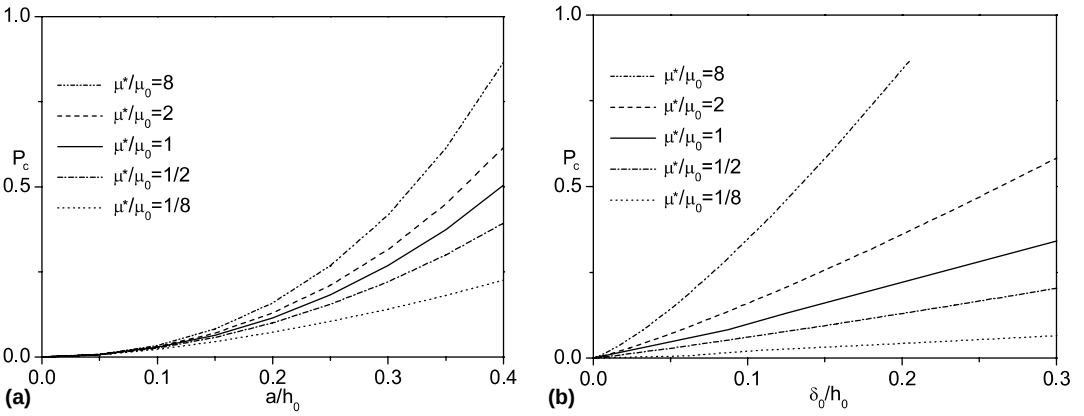


Fig. 12. The relations of $P_c$ vs $a$ (a) and $P_c$ vs $\delta_0$ (b) for various values of the stiffness ratio $\mu^*/\mu_0$ with $R/h_0 = 0.8$, the cylindrical stamp.

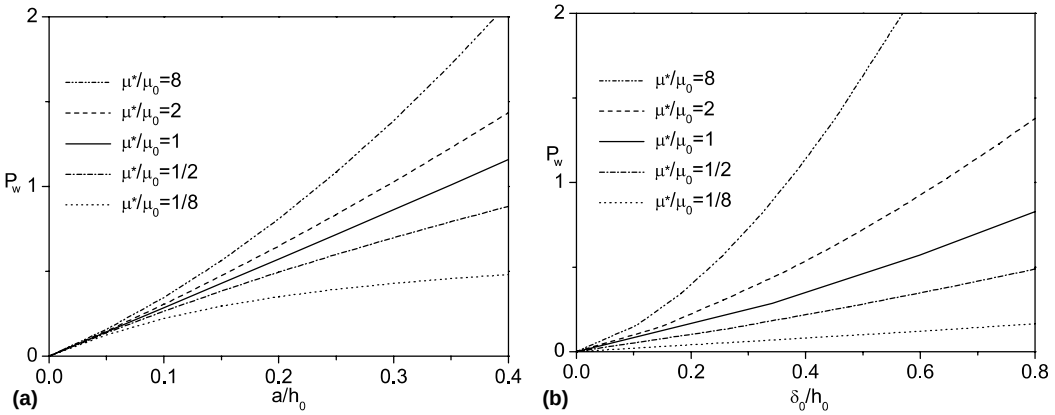


Fig. 13. The relations of $P_w$ vs $a$ (a) and $P_w$ vs $\delta_0$ (b) for various values of the stiffness ratio $\mu^*/\mu_0$, the wedge-shaped stamp.

As mentioned before, one of the advantages of the present model over others is that it can be used for the FGM with shear modulus varying arbitrarily and involves no discontinuity of the properties. As an example, we consider the shear modulus of coating varying in the following form:

$$\mu(y) = \mu^* + (\mu_0 - \mu^*)(y/h_0)^n. \tag{64}$$

where $n$ is a positive constant characterizing the gradual variation of the shear modulus. In the following calculation we also choose the number of the sub-layers to be 6. Here we use the present model to solve contact problems of flat, cylindrical and wedge-shaped stamps.

Figs. 14–16 illustrate the distributions of the contact pressure for some selected values of $n$ with fixed $\mu^*/\mu_0$ and $a/h_0$. Significant effects of the shear modulus gradient ($n$) of coatings are observed especially for the cylindrical (Fig. 15) and wedge-shaped (Fig. 16) stamps. With the increase of $n$, the contact pressure for the flat stamp decreases in most part of the contact area but increases in the area near two ends; while the contact pressure for the other two kinds of stamps increases in all contact area. This behavior implies that we can alter the distribution of the contact pressure by adjusting the gradient of the coating while remaining the stiffness of the coating surface unchanged.

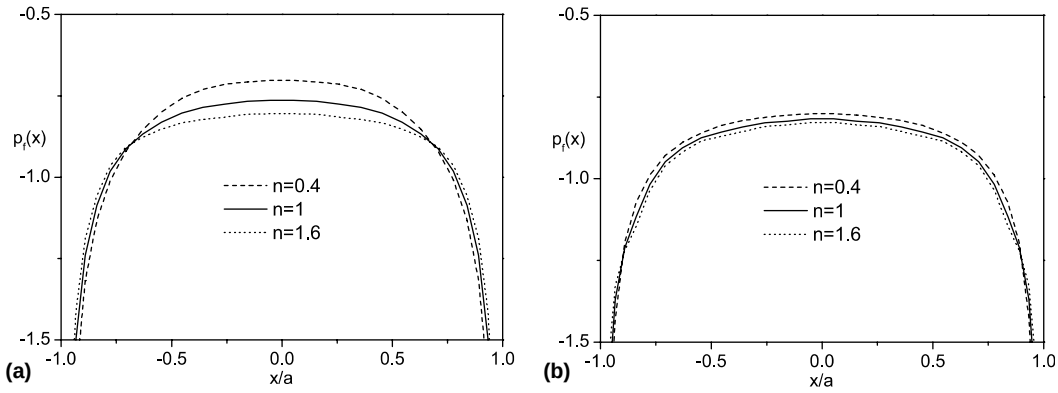


Fig. 14. The distribution of the contact pressure on the surface of FGM coating loaded by a flat stamp for various values of $n$, $\mu^*/\mu_0 = 8$: (a) $a/h = 0.1$ and (b) $a/h = 0.5$.

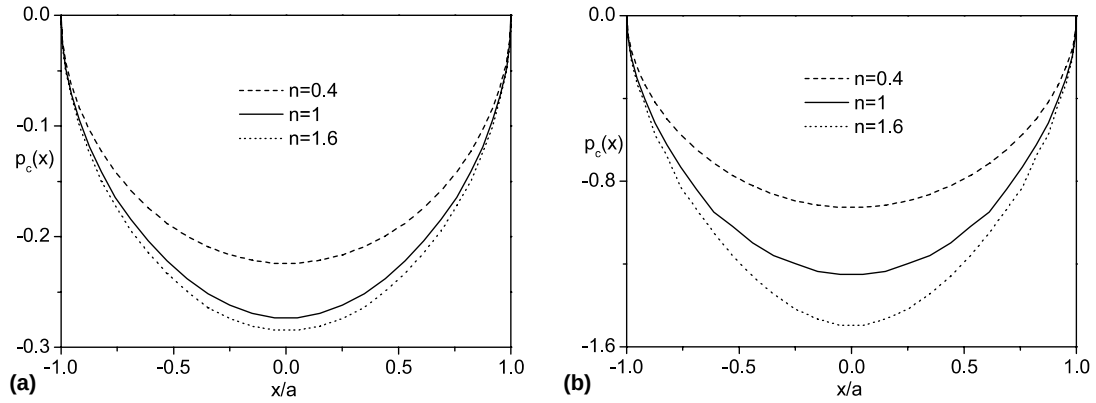


Fig. 15. The distribution of the contact pressure on the surface of FGM coating loaded by a cylindrical stamp for various values of $n$, $R/h = 0.8$, $\mu^*/\mu_0 = 8$: (a) $a/h = 0.1$ and (b) $a/h = 0.3$.

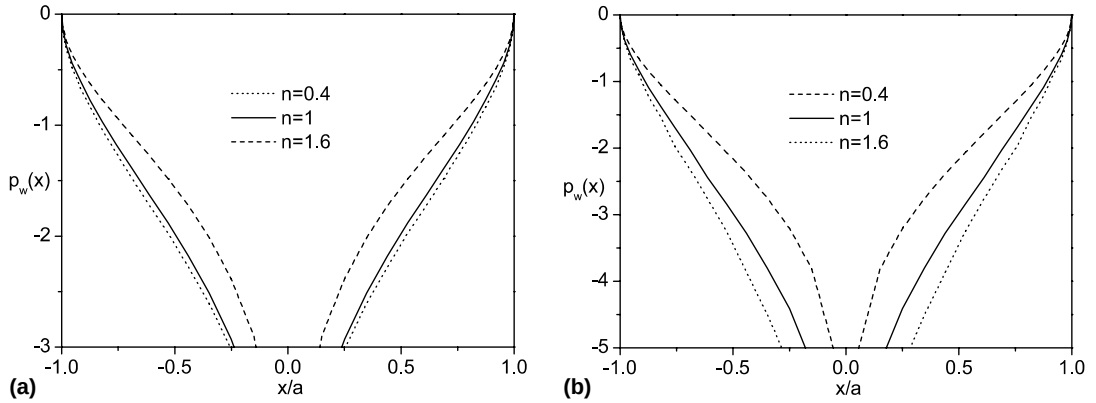


Fig. 16. The distribution of the contact pressure on the surface of FGM coating loaded by a wedge-shaped stamp for various values of $n$, $\mu^*/\mu_0 = 8$: (a) $a/h = 0.1$ and (b) $a/h = 0.3$.

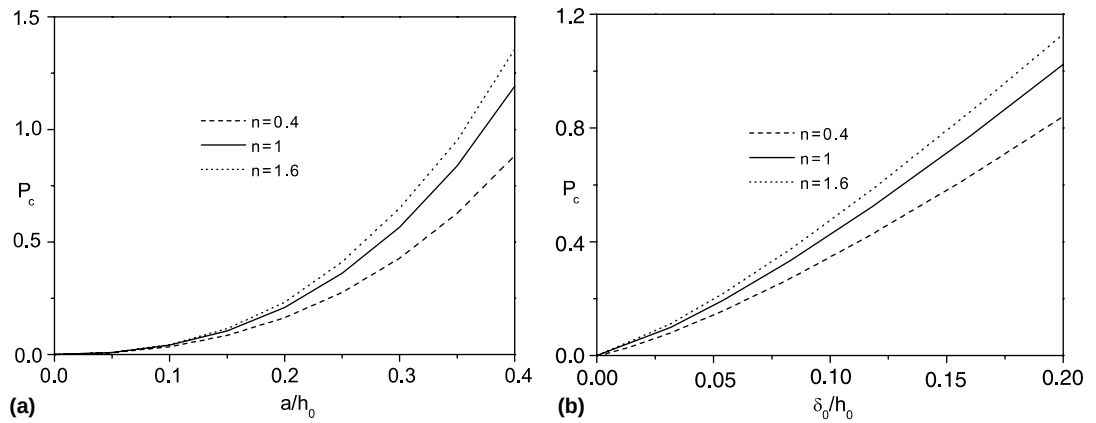


Fig. 17. The relations of $P_c$ vs $a$ (a) and $P_c$ vs $\delta_0$ (b) for various values of $n$, $R/h = 0.8$. $\mu^*/\mu_0 = 8$, the cylindrical stamp.

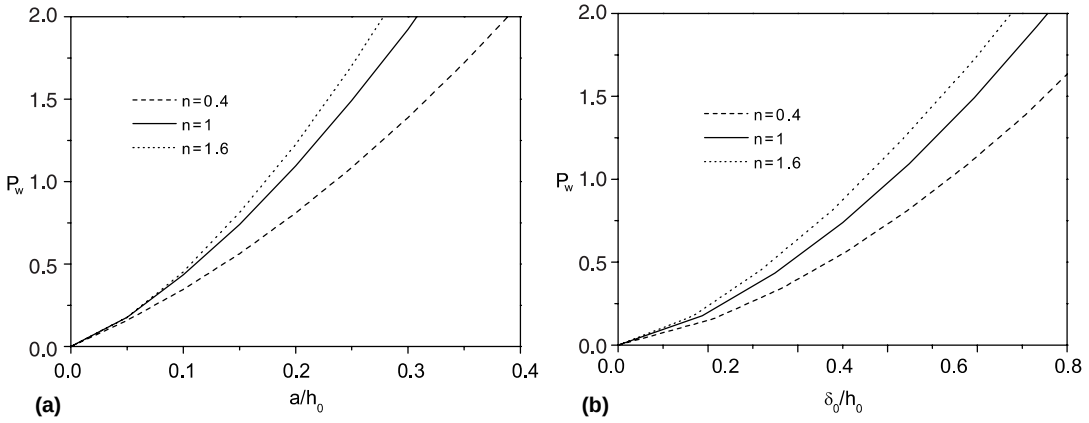


Fig. 18. The relations of $P_w$ vs $a$ (a) and $P_w$ vs $\delta_0$ (b) for various values of $n$, $\mu^*/\mu_0 = 8$, the wedge-shaped stamp.

The force-contact region ($P$–$a$) and force-indentation ($P$–$\delta_0$) relations are shown in Figs. 17 and 18 for some selected values of $n$ with fixed $\mu^*/\mu_0$ and $a/h_0$. All $P$–$a$ and $P$–$\delta_0$ curves are concave. To create the same contact region ($a$) and the same maximum indentation depth $\delta_0$, the larger applied normal load is needed for smaller values of $n$ because the gradual variation of the shear modulus can significantly alter the pressures around the stamp. The dependence of $P$–$\delta_0$ curves on the value of $n$ indicates that we can measure the gradient of the coating using the indentation-testing method even if the stiffness of the coating surface remain unchanged.

## 6. Concluding remarks

In the present paper, we have developed a multi-layered model for frictionless contact analysis of a functionally graded coating under plane strain-state deformation. The essence of the model is the approximation of the functionally graded material properties by a continuous but piecewise linear variation. To check the efficiency of the model, we have calculated the frictionless contact of the rigid flat, cylindrical, triangular and wedge-shaped stamps and compared the results with those of Guler and Erdogan's work. From the numerical results, we can find:

(1) The present model allows for arbitrary variation of the material properties.
(2) The present model is very efficient in solving the contact problem of the FGMs. Generally 4–6 sublayers can yield sufficiently accurate results.
(3) The distribution of the contact pressure can be altered by adjusting the gradient of the coating.
(4) The dependence of force-indentation relations on the gradients indicates that we can measure the gradient of the coating using the indentation-testing method.

Finally, we mention that the present work has many potential applications in geomechanics, biomechanics, thin films, coatings, and other engineered materials. Also, the results of this study can be useful in interpreting experiments and potentially for the design of materials themselves.

## Acknowledgement

Support by the National Science Foundation and Doctoral Science Fund of MOE under Grant No. 20020004005 is gratefully acknowledged.

## References

Dag, S., Erdogan, F., 2002. A surface crack in a graded medium loaded by a rigid stamp. Engng. Fract. Mech. 69, 1729–1751.
Erdogan, F., Gupta, G.D., 1972. On the numerical solution of singular integral equations. Quart. Appl. Math. 29, 525–534.
Giannakopoulos, A.E., Pallot, P., 2000. Two-dimension contact analysis of elastic graded materials. J. Mech. Phys. Solids 48, 1597–1631.
Giannakopoulos, A.E., Suresh, S., 1997a. Indentation of solids with gradients in elastic properties: Part I. Point force solution. Int. J. Solids Struct. 34, 2357–2392.
Giannakopoulos, A.E., Suresh, S., 1997b. Indentation of solids with gradients in elastic properties: Part II. Axisymetric indenters. Int. J. Solids Struct. 34, 2392–2428.
Guler, M.A., Erdogan, F., 2004. Contact mechanics of graded coatings. Int. J. Solids Struct. 41, 3865–3889.
Huang, G.Y., Wang, Y.S., Gross, D., 2003. Fracture analysis of a functionally graded coating: plane deformation. Eur. J. A/Solids 22, 535–544.
Huang, G.Y., Wang, Y.S., Yu, S.W., 2004. Fracture analysis of a functionally graded in interfacial zone under plane deformation. Int. J. Solids Struct. 41, 731–743.
Ioakimidis, N.I., 1980. The numerical solution of crack problems in plane elasticity in the case of loading discontinuities. Engng. Fract. Mech. 15, 709–716.
Johnson, K.L., 1985. Contact Mechanics. Cambridge University Press.
Jorgensen, O., Giannakopoulos, A.E., Suresh, S., 1998. Spherical indentation of composite laminates with controlled gradients in elastic anisotropy. Int. J. Solids Struct. 35, 5097–5113.
Krenk, S., 1975. On quadrature formulas for singular integral equations of the first and the second kind. Quart. Appl. Math. 33 (3), 225–232.
Krumova, K., Klingshirn, C., Haupet, F., Friedrich, K., 2001. Microhardness studies on functionally graded polymer composites. Compos. Sci. Technol. 61, 557–563.
Muskhelishvili, N.I., 1953. Singular Integral Equations. Noordhoff, Leiden.
Pender, D.C., Thompson, S.C., 2001. Gradients in elastic modulus for improved contact-damage resistance. Part II: The silicon nitride–silicon carbide system. Acta Mater. 49, 3263–3268.
Pender, D.C., Padture, N.P., Giannakopoulos, A.E., Suresh, S., 2001. Gradients in elastic modulus for improved contact-damage resistance. Part I: The silicon nitride–oxynitride glass system. Acta Mater. 49, 3255–3262.
Plevako, V.P., 1973. Equilibrium of a nonhomogeneous half-plane under the action of forces applied to the boundary. Appl. Math. Mech. 37, 858–866.
Slater, L.J., 1960. Confluent Hypergeometric Function. Cambridge University Press, Cambridge.
Suresh, S., 2001. Graded materials for resistance to contact deformation and damage. Science 292, 2447–2451.
Suresh, S., Mortensen, A., 1998. Fundamentals of Functionally Graded Materials: Processing and Thermomechanical Behavior of Graded Metals and Metal–Ceramic Composites. IOM Communications Ltd., London.
Suresh, S., Giannakopoulos, A.E., Alcala, J., 1997. Spherical indentation of compositionally graded materials: theory and experiments. Acta Mater. 45, 1307–1321.
Suresh, S., Olsson, M., Padture, N.P., Jitcharoen, J., 1999. Engineering the resistance to sliding-contact damage through controlled gradients in elastic properties at contact surfaces. Acta Mater. 47, 3915–3926.
Wang, Y.S., Gross, D., 2000. Analysis of a crack in a functionally gradient interface layer under static and dynamic loading. Key Engng. Mater. 183–187, 331–336.
Wang, Y.S., Huang, G.Y., Gross, D., 2003. On the mechanical modeling of functionally graded interfacial zone with a Griffith crack: plane deformation. J. Appl. Mech. 70, 676–680.
Wang, Y.S., Huang, G.Y., Gross, D., 2004. On the mechanical modeling of functionally graded interfacial zone with a Griffith crack: plane deformation. Int. J. Fracture 125, 189–205.